

Solar Water Splitting Combining a BiVO₄ Light Absorber with a Ru-Based Molecular Cocatalyst

Moreno de Respinis,[†] Khurram S. Joya,[‡] Huub J. M. De Groot,[‡] Francis D'Souza,[§] Wilson A. Smith,[†] Roel van de Krol,^{||} and Bernard Dam^{*,†}

[†]Department of Chemical Engineering, Materials for Energy Conversion and Storage, Faculty of Applied Sciences, Delft University of Technology, Julianalaan 139, 2600GA Delft, The Netherlands

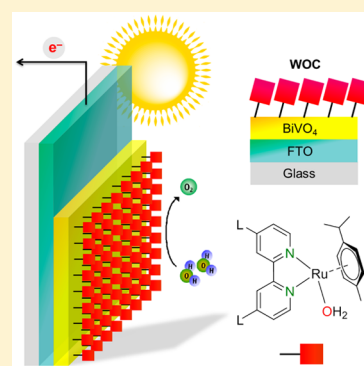
[‡]Leiden Institute of Chemistry, Leiden University, Einsteinweg 55, 2300RA Leiden, The Netherlands

[§]Department of Chemistry, University of North Texas, 1155 Union Circle, Denton, Texas 76203, United States

^{||}Helmholtz-Zentrum Berlin für Materialien und Energie GmbH, Institute for Solar Fuel, Hahn-Meitner-Platz 1, 14109 Berlin, Germany

Supporting Information

ABSTRACT: We demonstrate here for the first time the photoelectrochemical properties of a BiVO₄ photoanode in conjunction with a *molecular* catalyst. When the Ru-based molecular catalyst (RuCat) is coupled to a BiVO₄ light-absorber the performance of this photoanode improves particularly in the low-bias region (<1.0 V vs RHE). The RuCat-BiVO₄ photoanode shows a higher photocurrent than CoP_i-BiVO₄ under front illumination, and a 0.1 V more cathodic onset potential. The former can be partly explained by the low light absorption of the RuCat (<5% light absorption in the UV–vis–NIR range). For the latter, we propose that the linkers in the RuCat reduce the surface recombination in BiVO₄ to a greater extent than CoP_i. Finally, we observe that the fill factor of the RuCat-BiVO₄ JV characteristic improves after the stability test. The results presented herein not only show the feasibility and potential of the solid state/molecular heterojunctions but also represent a proof of principle to improve conventional all-solid-state systems such as CoP_i-BiVO₄.



1. INTRODUCTION

One of the challenges in solar water splitting is to control the semiconductor–electrolyte interface.^{1,2} In many cases, the presence of defects and traps results in high surface recombination rates.³ In addition, slow water oxidation kinetics often reduces the solar-to-chemical conversion efficiency. In order to optimize the light absorption in the solar spectrum, approaches with multiple bandgap heterojunction absorbers should be favored.⁴ To avoid losses, one needs to improve the photoanode efficiency at low applied bias. This can be achieved by nanostructuring,^{5–8} by the application of surface passivation layers,⁹ and by the decoration with an efficient surface catalyst.¹⁰ It is imperative to identify alternative catalysts or combinations of surface passivation layers and catalysts, that are able to reduce the recombination losses and enhance the reaction kinetics at a potential $V < 1$ V. In addition, the catalyst should not compete for the absorption of light with the semiconductor onto which it is deposited. While solid state heterojunctions have attracted much attention, molecular/solid state heterojunctions remain largely unexplored. Recent advances on molecular catalysts have made them highly efficient, with activities comparable to that of photosystem II.^{11–19} The focus on hybrid molecular/solid state approaches thus far has been mostly limited to the dye sensitized solar cell approach to water splitting, where light absorption was conducted by the

molecular compounds.^{20–22} Only recently a photoelectrode with an Fe-based molecular catalyst on WO₃ was demonstrated. In this case, the use of a molecular catalyst increased the current for photoelectrochemical water oxidation in non-neutral pH conditions, but the optical transparency and surface passivation effects of the catalyst were not considered.²³ In this study BiVO₄ is the semiconductor of choice due to the relatively deep understanding of its properties both in the particulate form,^{24–26} as well as in a thin film photoanode.^{27,28} Here we report for the first time the surface functionalization of BiVO₄ photoanodes with a molecular catalyst, a *p*-cymene ruthenium bipyridine aqua complex $[(\text{cy})\text{Ru}^{\text{II}}(\text{L}_2\text{bpy})\text{OH}_2]^+$ (L = linker 4,4'-dicarboxylic acid) that has a catalytic cycle with consecutive electron transfer events coupled to efficient proton release. This leads to redox leveling of catalytic intermediates and a narrow density of states localized at the catalyst.^{13–19} The proton NMR spectrum of the monoruthenium complexes is shown in Figure S1 (Supporting Information). For simplicity, undoped BiVO₄ samples are used in this study. We examine the performance of this planar molecular–solid state hybrid system in conjunction with all-solid-state systems such as the well-studied CoP_i-BiVO₄

Received: January 11, 2015

Revised: March 6, 2015

Published: March 6, 2015

in which CoP_i has been shown to be one of the most effective cocatalysts,²⁹ and RuO₂-BiVO₄. In addition, we compare their functionality to the case where the same catalysts are used as electrocatalysts on FTO.

2. EXPERIMENTAL DETAILS

(Photo)electrochemical Measurements. As a photoanode, we synthesized 200 nm dense films of BiVO₄ by spray pyrolysis. The spray deposition rate is ~1 nm per 5 s (1 cycle). The recipe for the preparation of the precursor solution and the spray pyrolysis setup are described elsewhere.^{10,29} Before every deposition, ~80 nm of SnO₂ layer was deposited onto FTO substrate to prevent recombination of electrons and holes at the FTO/BiVO₄ interface.²⁸ The substrates used are TEC-15 FTO-coated glass (15Ω/sq; Hartford Glass Co.). After the deposition, all samples were annealed for 2 h at 450 °C in air to further improve the crystallinity. A 30 nm CoP_i catalyst was electrodeposited according to the recipe from Kanan and Nocera.³⁰ The electrodeposition was performed at a constant voltage of 1.7 V versus RHE for 15 min. Care was taken to always keep the electrodeposited CoP_i layer wet, as intermediate drying of the CoP_i was found to adversely affect the stability. The BiVO₄ photoanodes and the FTO anodes were functionalized with molecular water oxidation catalyst by immobilizing the *p*-cymene ruthenium derived bipyridine complex [(cy)Ru^{II}(L₂bpy)OH₂]⁺. The catalyst was dispersed into an aqueous solution, and the deposition was obtained by dip-coating the substrates into the catalyst solution for periods of 1.5–3 h. RuO₂ NPs were synthesized by the solvothermal method and calcined in air at 300 °C for 3 h.³¹ An aqueous solution (2 mL) of catalyst (5 mg) was prepared and mixed in an ultrasonic bath. A 20 μL portion of aqueous solution of catalyst was deposited on the FTO or BiVO₄ substrates. Photoelectrochemical characterization was carried out in an aqueous 0.1 M potassium phosphate electrolyte solution (pH ~7.1). The solution was purged with nitrogen prior and during the measurements to remove any dissolved oxygen. The working area of the electrodes exposed to the electrolyte was 28.3 mm² (6 mm diameter) for all samples. The potential of the working electrode was controlled by a potentiostat (EG&G PAR 283). In three-electrode measurements, a coiled Pt wire and an Ag/AgCl electrode (XR300, saturated KCl and AgCl solution; Radiometer Analytical) were used as the counter and reference electrodes, respectively. Cyclic voltammetry measurements were performed with a scan rate of 50 mV s⁻¹. White light photocurrent measurements were performed under simulated AM1.5 solar illumination (100 mW cm²) with a Newport Sol3A Class AAA solar simulator (type 94023 ASR3). Electrical contact to the sample was made using a silver wire and graphite paste. A Keithley 2001 multimeter was used as the ammeter in the current versus time measurements, and as an auxiliary high-impedance voltmeter (>10 GΩ) connected to the working (WE) and counter (CE) electrodes to measure the two-electrode voltage. The UV–vis–NIR absorption was measured with a balanced deuterium-halogen lamp as the light source and a Maya 2000 spectrophotometer as the detector.

Electrochemical Quartz Crystal Nanobalance. EQCN experiments, with simultaneous cyclic voltammetry and piezoelectric gravimetry measurements, were performed with an Elchema EQCN-600 nanobalance and an Elchema PS-605B potentiostat. Both instruments were computer-controlled with the Elchema Voltscan program (version V.4.1). A conventional

three-electrode cell configuration was used; the counter electrode was a platinum foil, and an Ag/AgCl/KCl electrode (Bioanalytical Systems, Inc.) served as the reference. The working electrode was a 14 mm diameter quartz crystal (AT cut, plano–plano, 10 MHz) coated with a gold/chromium conducting surface (approximate electroactive surface area: 0.256 cm²). The quartz crystal disc was mounted in an EQCM-5710 quartz crystal holder from the Polish Academy of Sciences. The frequency response of the quartz crystal was additionally monitored before and during experiments using a Fluke PM6680B high-resolution frequency counter.

Synthesis of the Catalyst Complexes. *Chloro Complex [(cy)Ru^{II}(L₂bpy)Cl]Cl.* 4,4'-Dicarboxylic acid-2,2'-bipyridine (L₂bpy: 0.244 g, 1.0 mmol) was dissolved in 0.5 mL of water containing NaOH (0.08 g, 2.0 mmol), and MeOH (25 mL) was added to it. This mixture was poured into a stirred mixture of [RuCl₂(*p*-cymene)]₂ dimer (0.362 g, 0.5 mmol) in absolute MeOH (20 mL). The whole reaction mixture was further stirred for 2 h at 40–45 °C. The solution was cooled to room temperature, and the pH was lowered to 1–2 by addition of 0.5 M HCl. The free ligand was filtered off, and the solvent mixture was evaporated under vacuum. The solid orange chloro complex [(cy)Ru^{II}(L₂bpy)Cl]Cl thus obtained was reprecipitated from MeOH or acetone by addition of ether/hexane. Yield 0.43 g, 78%. ¹H NMR (CD₃OD, 295 K, δ ppm, J Hz): 9.66 (d, 2H, H^{6,6'}_{dcabpy}, J 5.76); 8.99 (s, 2H, H^{3,3'}_{dcabpy}); 8.22 (dd, 2H, H^{5,5'}_{dcabpy}, J 1.49, J 5.79); 6.19 (d, 2H, Ar_{*p*-cy}, J 6.33); 5.95 (d, 2H, Ar_{*p*-cy}, J 6.33); 2.66 (sep, 1H, –CH(CH₃)_{2*p*-cy}); 2.27 (s, 3H, CH_{3*p*-cy}); 1.06 (d, 6H, –CH(CH₃)_{2*p*-cy}, J 6.91). Anal. Found: C, 45.56%; H, 4.41%; N, 4.85%. Calcd: C, 45.74%; H, 4.36%; N, 4.86% for C₂₂H₂₂N₂O₄Ru₁Cl₂·1.5H₂O complex.

Catalyst Complex [(cy)Ru^{II}(L₂bpy)–OH₂]²⁺ (RuCat). The chloro complex [(cy)Ru^{II}(L₂bpy)Cl]Cl was converted into the aqua (OH₂) catalyst [(cy)Ru^{II}(L₂bpy)–OH₂]²⁺ by stirring with aqueous solution containing 2.1 equiv of AgNO₃ or silver hexafluorophosphate in methanol (1:1, H₂O/MeOH) for 30 min. The white precipitates were filtered off, and the solvent mixture was evaporated under vacuum. The yellow solid aqua complex thus obtained was reprecipitated from acetone or MeOH by addition of ether/hexane.

RuCat Deposition. [RuCl₂(*p*-cymene)]₂ dimer and RuCl₃·*n*H₂O were obtained from Sigma-Aldrich Co., and used as received. L₂bpy (4,4'-diphosphonic acid-2,2'-bipyridine) was prepared using literature procedures.^{32,33} Unless otherwise specified, the solutions were prepared in ultrapure water (Millipore Milli-Q A10 gradient, 18.2 MΩ cm, 2–4 ppb total organic content). Compounds, ligands, and catalyst complexes were synthesized in argon/nitrogen atmosphere. The glassware and the electrochemical cell were cleaned as described previously.³⁴ Proton NMR spectra were obtained with a Bruker WM-300 MHz spectrophotometer. Immobilization of the catalyst on FTO coated glass slides (1 × 2.5 cm²), and BiVO₄ coated FTO was carried out according to our previously described procedure.³⁵

3. RESULTS AND DISCUSSION

In this study, we choose to perform all (photo)electrochemical measurements at pH 7.1 in 0.1 M phosphate buffer, conditions under which the performance and stability of the CoP_i are optimal. A study on the effect of the electrolyte anions and pH may reveal conditions under which the performance of RuCat is even higher than herein reported. First we compared the

electrocatalytic activity for water oxidation on the bare FTO substrate, with that for FTO coated with CoP_i , RuO_2 , and the RuCat catalysts, as shown in Figure 1. The cyclic voltammetry

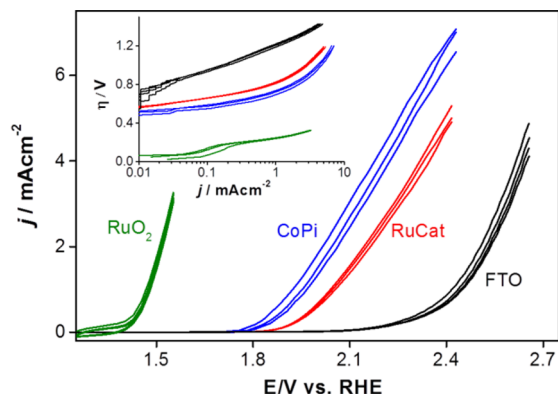


Figure 1. JV curve for RuCat@FTO (red), CoP_i @FTO (blue), RuO_2 @FTO (green), and bare FTO (black). The inset is the Tafel plot. Measurements performed at 50 mV s^{-1} .

gram shows that RuO_2 has the lowest onset potential ($V_{\text{on}} = \sim 1.4 \text{ V vs RHE}$), while for CoP_i and RuCat a negligible current is flowing through the cell up to an applied potential of 1.75 V versus RHE. The potential for the reversible water oxidation reaction is at 1.23 V versus RHE, which implies an overpotential of 0.7 and 0.8 V at 1 mA cm^{-2} for CoP_i and RuCat, respectively. We conclude that RuCat is not the most active electrocatalyst on FTO.

Next, we studied the light driven water oxidation catalysis in conjunction with a BiVO_4 light absorber. Figure 2 shows the

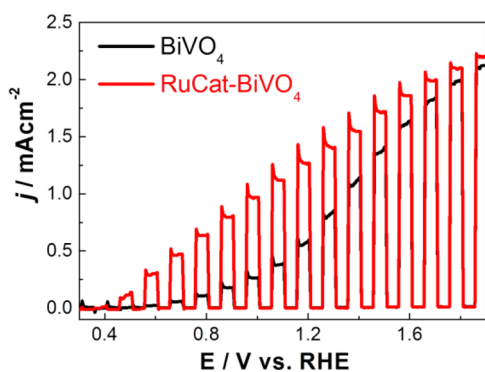


Figure 2. JV curve for a bare BiVO_4 (black), and for Ru-catalysts on BiVO_4 (red). Measurement performed at 10 mV/s , under chopped AM 1.5 back illumination.

linear sweep voltammogram under chopped illumination for a BiVO_4 photoanode with and without anchoring the RuCat. The photocurrent density of the RuCat- BiVO_4 photoanode increases at all potentials. The enhancement is most pronounced at low potential, resulting in an improved fill factor of the polarization curve. The improved fill factor for the RuCat- BiVO_4 system can be attributed to reduced surface recombination, enhanced charge injection (i.e., oxygen evolution kinetics), or both. In fact, the more pronounced current transients between 0.6 and 1.7 V for the RuCat- BiVO_4 suggest that the photogenerated charges live longer.²⁹ This favors an explanation in terms of reduced surface recombination at low current density. It is also corroborated by the

absence of cathodic transients when the light is turned off, which would indicate an accumulation of holes at the semiconductor–catalyst interface due to slow catalysis. The fact that the photocurrent improves at low potentials, but not at higher potentials, is fully consistent with the explanation that the photocurrent is limited by surface states. For unmodified BiVO_4 at low potentials, electrons in the conduction band may be injected into the surface states, so passivation of these states would help. At higher applied potentials, conduction band electrons are more strongly driven away from the surface, and cannot reach the surface states anymore. Therefore, passivation of the surface states does not help at these potentials.³⁶ All in all we find that the current density for the RuCat- BiVO_4 is 5.5 times higher than the one for bare BiVO_4 at 0.8 V versus RHE, where 0.8 V is a typical operating voltage when using this anode in conjunction with, e.g., a single junction amorphous silicon solar cell. The improved JV characteristic is a sign that RuCat has been successfully deposited, since the presence of RuCat enhances the oxidative power of the substrate. At this stage, however, the exact nature and structure of the RuCat during catalysis in a phosphate buffer is unknown. The characterization of the BiVO_4 –RuCat interface will be the subject of further work.

Figure 3A,B shows the current density of RuCat- BiVO_4 and CoP_i - BiVO_4 under continuous frontside and backside illumination. Interestingly, in both configurations the onset potential (V at 0.1 mA cm^{-2}) for RuCat- BiVO_4 is comparable to that for CoP_i - BiVO_4 . In contrast, the electrocatalytic measurements in Figure 1 show that CoP_i @FTO has a lower onset for water oxidation than RuCat@FTO. Comparable results are obtained in the dark with RuCat or CoP_i deposited on BiVO_4 instead of FTO (Supporting Information Figure S2). This apparent contradiction suggests that the cathodic shift in the onset potential for the RuCat- BiVO_4 is not due to enhanced water oxidation catalysis, but to reduced surface recombination (since surface recombination does not play a role in the electrocatalytic experiments shown in Figure 1). The cathodic shift in onset potential between the electrocatalysis (Figure 1) and the photoelectrocatalysis (Figure 3A,B) is related to the photovoltage of BiVO_4 . In order to get the highest photovoltage out of a semiconductor (and therefore the smallest V_{on} under illumination), it is favorable for the hole quasi-Fermi level $E_{\text{F,h}}$ to equilibrate as closely as possible to the valence band top, and the electron quasi-Fermi level $E_{\text{F,e}}$ as closely as possible to the conduction band bottom. To understand this concept, one needs to consider that the photovoltage of a semiconductor in an aqueous medium is often limited by the Fermi-level pinning due to recombination at surface states (Figure 5A). By passivating these surface states through the application of a suitable catalyst such as CoP_i , the $E_{\text{F,h}}$ becomes unpinned resulting in a higher photovoltage ΔV_{photo} , which is then limited by recombination of conduction band electrons with the holes accumulating in the catalyst (Figure 5B). It has been shown that CoP_i effectively passivates the surface states in Fe_2O_3 and promotes near-complete suppression of surface recombination in BiVO_4 .^{37–39} The comparable onset potential of the RuCat- BiVO_4 presumably means that the RuCat is as effective as CoP_i in passivating the BiVO_4 surface states. In the case of RuCat, possibly the recombination is further reduced by its linkers which increase the distance (introduce a tunneling barrier) between the conduction band electrons and the holes accumulating in the reaction center (Ru), which in turn increases the $E_{\text{F,h}}$ (Figure 5C). Note that the molecular catalyst

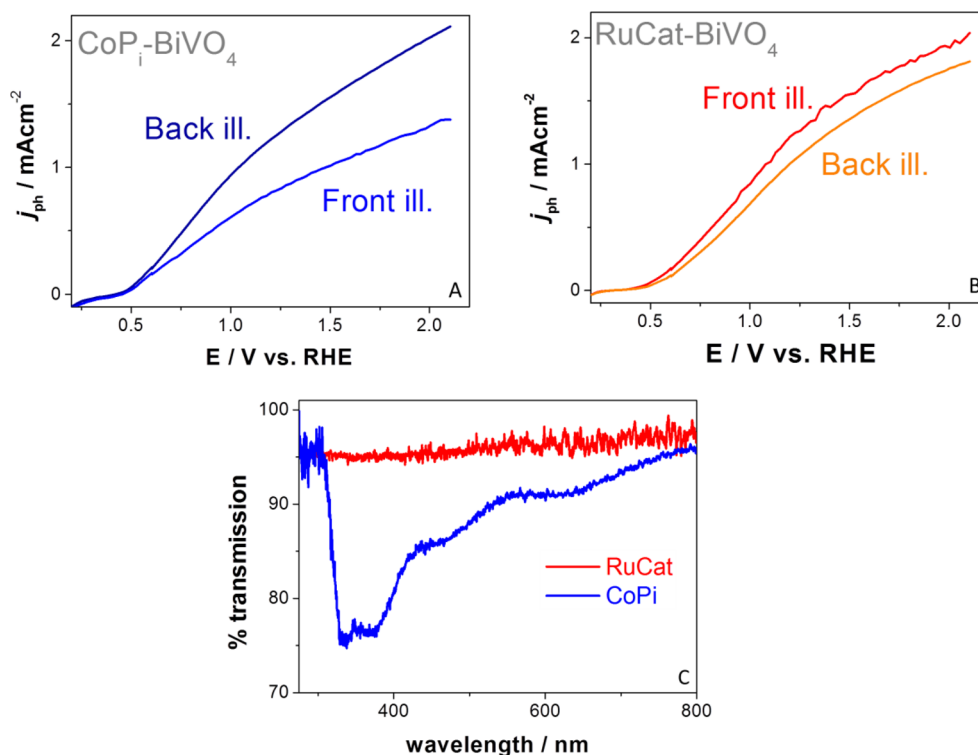


Figure 3. *JV* scans for $\text{CoP}_i\text{-BiVO}_4$ (A) and RuCat-BiVO_4 (B) under front illumination (light from the electrolyte/catalyst interface) and under back illumination (light from the FTO-glass). Transmission spectrum for $\text{CoP}_i\text{@FTO}$ as recorded at the end of the deposition is compared with the ex-situ UV-vis spectrum for RuCat on glass (C). The strong absorbance of the FTO precludes the measurement at wavelengths below 330 nm. CoP_i deposition done in potentiostatic mode at 1.7 V vs RHE. In 900 s a 30 nm thin film has deposited, which is the optimal thickness for CoP_i -catalyzed BiVO_4 .¹⁰

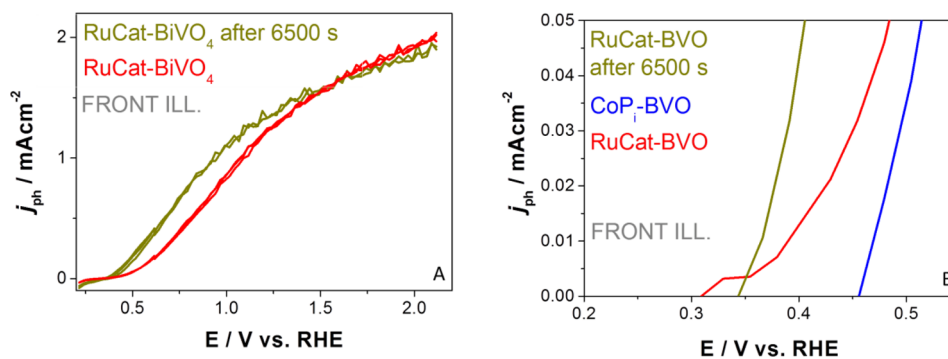


Figure 4. *JV* scans before and after 2.5 h of reaction under illumination for a RuCat-catalyzed BiVO_4 (A). *JV* scans for a CoP_i -catalyzed BiVO_4 and RuCat-catalyzed BiVO_4 . For RuCat- BiVO_4 the *JV* after the stability test is compared. Measurements performed at 50 mV s^{-1} under front illumination (light from the electrolyte/catalyst interface) (B).

is expected to be both ion-permeable and redox-active, which leads to the formation of a so-called *adaptive junction*.⁴⁰ In such a junction, the oxidation of a catalyst intermediate increases its redox potential (i.e., it lowers the catalyst electrochemical potential) and thus lowers the $E_{F,h}$. This also contributes to an increase in ΔV_{photo} .

We observe that V_{on} for $\text{CoP}_i\text{-BiVO}_4$ under front illumination is slightly more anodic than under back illumination (Supporting Information Figure S4), and the saturation current density is lower in the former (Figure 3A). These differences do not occur in RuCat-BiVO_4 (Figure 3B and Supporting Information Figure S4) and can be attributed to the parasitic light absorption by the CoP_i . Our UV-vis measurements of the $\text{CoP}_i\text{@FTO}$, compared with the absorption through the RuCat, are shown in Figure 3C. CoP_i absorbs up to 25% of the light at

wavelengths shorter than the bandgap of BiVO_4 while RuCat only absorbs 5%. It was shown that Co^{IV} species are formed at potentials positive of 1.5 V versus RHE,⁴¹ and that they are characterized by dark coloration.⁴² Thus, those are the species formed when we deposit the CoP_i film at 1.7 V versus RHE, and the ones which are required to evolve oxygen.⁴¹

The stabilities of the $\text{CoP}_i\text{-BiVO}_4$ and RuCat-BiVO_4 samples at 1.23 V versus RHE, under AM1.5 illumination, were measured over a period of 6500 s as shown in Supporting Information Figure S3 (top). While the photoanode performance under constant bias and illumination is slowly degrading over time, we observe that the cyclic voltammogram under illumination of the RuCat-BiVO_4 samples after the stability test shows an improved fill factor compared to a freshly made sample (Figure 4A). In this experiment, for each cyclic

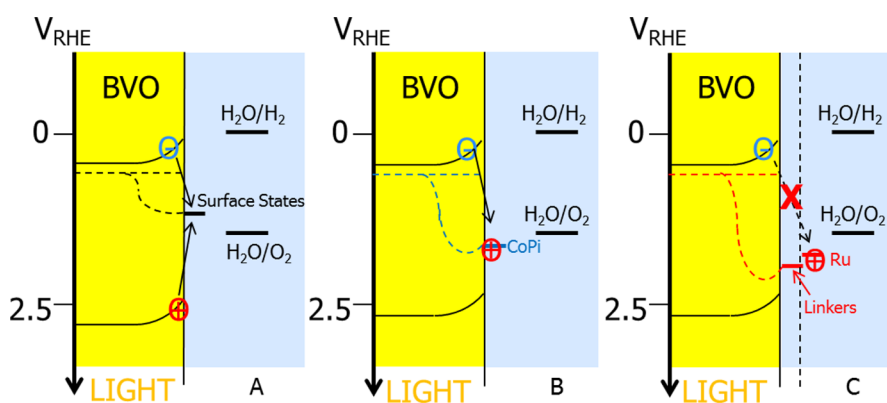


Figure 5. Schematic energy diagram under reaction conditions (low applied bias) including the conduction and valence bands, the quasi-Fermi levels of BiVO_4 in the dark and under illumination, in the presence of surface states and with a catalyst; the redox level of the CoPi catalyst and the Ru-based molecular complex; the redox potential for water oxidation. (A) Photovoltage and recombination at surface states on an uncatalyzed BiVO_4 . (B) Passivation of surface states, increased photovoltage, and recombination on Co sites in CoPi-BiVO_4 . (C) Further increased photovoltage and reduced recombination on RuCat-BiVO_4 .

voltammetry three cycles are taken. As those cycles overlap, we can say that between them there is no evidence for degradation. Given the limited thickness of the as-deposited RuCat catalyst, this strongly suggests that the observed photocurrent is due to oxygen evolution rather than catalyst degradation.

The reason for the fill factor improvement is unclear; however, reasonable interpretations could be a reduced surface recombination due to an improved semiconductor/catalyst interface, or improved catalysis over the RuCat . The latter explanation is supported by the electrocatalytic measurements before and after the stability test shown in Supporting Information Figure S3B, where the dark currents of the RuCat-BiVO_4 and RuCat@FTO slightly increase after the stability test. By zooming in around the V_{on} , we observe that after the stability test V_{on} is at around 0.35 V versus RHE, unchanged compared to before the stability test. Moreover we observe that this value is 0.1 V more cathodic than for CoPi-BiVO_4 (Figure 4B). This difference further supports our interpretation of reduced surface recombination as compared to CoPi . To exclude the possibility that the improvement after the continuous reaction is due to the oxidation of RuCat to RuO_x , we deposited RuO_2 onto BiVO_4 for comparison. In fact, in Supporting Information Figure S6 we observe that the photocurrents for $\text{RuO}_2\text{-BiVO}_4$ are significantly lower than for RuCat-BiVO_4 . Furthermore, a comparison of Figure 3 and Supporting Information Figure S6 shows that while RuO_2 NPs are excellent catalysts for the electrocatalytic oxidation of water, they do not enhance the photoelectrocatalytic performance of BiVO_4 . Finally, we tested the molecular integrity of RuCat by *in situ* electrochemical quartz crystal nanobalance (EQCN) experiments (Supporting Information Figure S5). The EQCN data reveal only small reversible mass changes and show no sign of persistent mass gain in the potential window for water oxidation.

4. CONCLUSIONS

In summary, we explored the (photo)electrochemical performance of BiVO_4 photoanodes for water oxidation modified with a ruthenium derived aqua complex $[(\text{cy})\text{Ru}^{\text{II}}(\text{bpy})\text{OH}_2]^+$ molecular catalyst (RuCat). We find that the electrocatalytic activity of a catalyst cannot be used to determine its effectiveness as a cocatalyst, since RuCat and CoPi outperform RuO_2 as a cocatalyst for BiVO_4 photoanodes. The limited thickness of the

molecular catalyst results in a light absorption of only 5% across the UV–vis–NIR spectrum, which allows for a higher saturation current density under front illumination as compared to CoPi . In addition, we find that the RuCat-BiVO_4 photoanode shows a 0.1 V more cathodic onset potential compared to CoPi-BiVO_4 . This we attribute to the larger distance between the conduction band electrons and the reaction center (Ru). Finally, while the photocurrent at constant potential is slowly decreasing in time, we observe that the fill factor of the RuCat-BiVO_4 JV -characteristic improves after the stability test. Electrocatalytic measurements suggest an improved catalysis over the RuCat ; however, a reduced surface recombination due to an improved semiconductor/catalyst interface could also contribute. The improved fill factor, the smaller onset potential, and the enhanced stability make the use of such a molecular catalyst an interesting proposition when designing a heterojunction tandem device where light must first pass through the catalyst layer.

■ ASSOCIATED CONTENT

Supporting Information

Additional figures, including NMR data and JV scans. This material is available free of charge via the Internet at <http://pubs.acs.org>.

■ AUTHOR INFORMATION

Corresponding Author

*E-mail: B.Dam@tudelft.nl.

Notes

The authors declare no competing financial interest.

■ ACKNOWLEDGMENTS

This research is financed in part by the BioSolar Cells open innovation consortium, supported by the Dutch Ministry of Economic Affairs, Agriculture and Innovation. K.S.J. acknowledges research funding from the Higher Education Commission (HEC), Government of Pakistan. M.d.R. acknowledges the work by Ronald van Schie on the open circuit voltage measurements.

■ REFERENCES

(1) van de Krol, R.; Grätzel, M. *Photoelectrochemical Hydrogen Production*; Springer: New York, 2012.

- (2) Joya, K. S.; Faheem, Y.; Ocakoglu, K.; van de Krol, R. Water-Splitting Catalysis and Solar Fuel Devices: Artificial Leaves on the Move. *Angew. Chem., Int. Ed.* **2013**, *52*, 10426–10437.
- (3) Sivula, K. Metal Oxide Photoelectrodes for Solar Fuel Production, Surface Traps, and Catalysis. *J. Phys. Chem. Lett.* **2013**, *4*, 1624–1633.
- (4) Abdi, F. F.; Han, L.; Smets, A. H. M.; Zeman, M.; Dam, B.; van de Krol, R. Efficient Solar Water Splitting by Enhanced Charge Separation in a Bismuth Vanadate-Silicon Tandem Photoelectrode. *Nat. Commun.* **2013**, *4*, 2195.
- (5) van de Krol, R.; Liang, Y.; Schoonman, J. Solar Hydrogen Production with Nanostructured Metal Oxides. *J. Mater. Chem.* **2008**, *18*, 2311–2320.
- (6) Osterloh, F. E. Inorganic Nanostructures for Photoelectrochemical and Photocatalytic Water Splitting. *Chem. Soc. Rev.* **2013**, *42*, 2294–2320.
- (7) de Respinis, M.; De Temmerman, G.; Tanyeli, I.; van de Sanden, M. C. M.; Doerner, R. P.; Baldwin, M. J.; van de Krol, R. Efficient Plasma Route to Nanostructure Materials: Case Study on the Use of m-WO₃ for Solar Water Splitting. *ACS Appl. Mater. Interfaces* **2013**, *5*, 7621–7625.
- (8) Maijenburg, A. W.; Hattori, A. N.; de Respinis, M.; McShane, C. M.; Choi, K.-S.; Dam, B.; Tanaka, H.; ten Elshof, J. E. Ni and p-Cu₂O Nanocubes with a Small Size Distribution by Templated Electrodeposition and Their Characterization by Photocurrent Measurement. *ACS Appl. Mater. Interfaces* **2013**, *5*, 10938–10945.
- (9) Liang, Y.; Messinger, J. Improving BiVO₄ Photoanodes for Solar Water Splitting through Surface Passivation. *Phys. Chem. Chem. Phys.* **2014**, *16*, 12014–12020.
- (10) Abdi, F. F.; Firet, N.; van de Krol, R. Efficient BiVO₄ Thin Film Photoanodes Modified with Cobalt Phosphate Catalyst and W-doping. *ChemCatChem* **2013**, *5*, 490–496.
- (11) Duan, L.; Bozoglian, F.; Mandal, S.; Stewart, B.; Privalov, T.; Llobet, A.; Sun, L. A Molecular Ruthenium Catalyst with Water-Oxidation Activity Comparable to that of Photosystem II. *Nat. Chem.* **2012**, *4*, 418–423.
- (12) Tong, L.; Duan, L.; Xu, Y.; Privalov, T.; Sun, L. Structural Modifications of Mononuclear Ruthenium Complexes: A Combined Experimental and Theoretical Study on the Kinetics of Ruthenium-Catalyzed Water Oxidation. *Angew. Chem., Int. Ed.* **2011**, *50*, 445–449.
- (13) Vallés-Pardo, J. L.; Guijt, M. C.; Iannuzzi, M.; Joya, K. S.; de Groot, H. J. M.; Buda, F. Ab Initio Molecular Dynamics Study of Water Oxidation Reaction Pathways in Mono-Ru Catalysts. *ChemPhysChem* **2012**, *13*, 140–146.
- (14) Joya, K. S.; de Groot, H. J. M. Efficient Water Splitting by Single Site Ruthenium Catalyst. *Eur. Conf. Chem. Life Sci., 4th* **2011**, 51–54.
- (15) Joya, K. S. Molecular Catalytic System for Efficient Water Splitting. Ph.D. Thesis, Leiden University, The Netherlands, 2011.
- (16) Joya, K. S.; Vallés-Pardo, J. L.; Joya, Y. F.; Eisenmayer, T.; Thomas, B.; Buda, F.; de Groot, H. J. M. Molecular Catalytic Assemblies for Electrodriven Water Splitting. *ChemPlusChem* **2013**, *78*, 35–47.
- (17) Joya, K. S.; de Groot, H. J. M. Artificial Leaf Goes Simpler and More Efficient for Solar Fuel Generation. *ChemSusChem* **2014**, *7*, 73–76.
- (18) Joya, K. S.; Joya, Y. F.; de Groot, H. J. M. Ni-Based Electrocatalyst for Water Oxidation Developed In-Situ in a HCO₃⁻/CO₂ System at Near-Neutral pH. *Adv. Energy Mater.* **2014**, *4*, 1301929 DOI: 10.1002/aenm.201301929.
- (19) Joya, K. S.; Takanabe, K.; de Groot, H. J. M. Surface Generation of a Cobalt-Derived Water Oxidation Electrocatalyst Developed in a Neutral HCO₃⁻/CO₂ System. *Adv. Energy Mater.* **2014**, DOI: 10.1002/aenm.201400252.
- (20) Swierk, J. R.; Mallouk, T. E. Design and Development of Photoanodes for Water-Splitting Dye-Sensitized Photoelectrochemical Cells. *Chem. Soc. Rev.* **2013**, *42*, 2357.
- (21) Jiao, F.; Frei, H. Nanostructured Cobalt Oxide Clusters in Mesoporous Silica as Efficient Oxygen-Evolving Catalysts. *Angew. Chem.* **2009**, *121*, 1873–1876.
- (22) Zhang, M.; de Respinis, M.; Frei, H. M. Time-Resolved Observations of Water Oxidation Intermediates on a Cobalt Oxide Nanoparticle Catalyst. *Nat. Chem.* **2014**, *6*, 362–367.
- (23) Klepser, B. M.; Bartlett, B. M. Anchoring a Molecular Iron Catalyst to Solar-Responsive WO₃ Improves the Rate and Selectivity of Photoelectrochemical Water Oxidation. *J. Am. Chem. Soc.* **2014**, *136* (5), 1694–1697.
- (24) Tokunaga, S.; Kato, H.; Kudo, A. Selective Preparation of Monoclinic and Tetragonal BiVO₄ with Scheelite Structure and Their Photocatalytic Properties. *Chem. Mater.* **2001**, *13*, 4624–4628.
- (25) Yu, J.; Kudo, A. Effects of Structural Variation on the Photocatalytic Performance of Hydrothermally Synthesized BiVO₄. *Adv. Funct. Mater.* **2006**, *16*, 2163–2169.
- (26) Aiga, N.; Jia, Q.; Watanabe, K.; Kudo, A.; Sugimoto, T.; Matsumoto, Y. Electron-Phonon Coupling Dynamics at Oxygen Evolution Sites of Visible-Light-Driven Photocatalyst: Bismuth Vanadate. *J. Phys. Chem. C* **2013**, *117*, 9881–9886.
- (27) Abdi, F. F.; Savenije, T. J.; May, M. M.; Dam, B.; van de Krol, R. The Origin of Slow Carrier Transport in BiVO₄ Thin Film Photoanodes: A Time-Resolved Microwave Conductivity Study. *J. Phys. Chem. Lett.* **2013**, *4*, 2752–2757.
- (28) Liang, Y. Q.; Tsubota, T.; Mooij, L. P. A.; van de Krol, R. Highly Improved Quantum Efficiencies for Thin Film BiVO₄ Photoanodes. *J. Phys. Chem. C* **2011**, *115*, 17594–17598.
- (29) Abdi, F. F.; van de Krol, R. Nature and Light Dependence of Bulk Recombination in Co-Pi-Catalyzed BiVO₄ Photoanodes. *J. Phys. Chem. C* **2012**, *116* (17), 9398–9404.
- (30) Kanan, M. W.; Nocera, D. G. In Situ Formation of an Oxygen-Evolving Catalyst in Neutral Water Containing Phosphate and Co²⁺. *Science* **2008**, *321*, 1072–1075.
- (31) Cruz, J. C.; Baglio, V.; Siracusano, S.; Antonucci, V.; Aricò, A. S.; Ornelas, R.; Ortiz-Frade, L.; Osorio-Monreal, G.; Durón-Torres, S. M.; Arriaga, L. G. Preparation and Characterization of RuO₂ Catalysts for Oxygen Evolution in a Solid Polymer Electrolyte. *Int. J. Electrochem. Sci.* **2011**, *6*, 6607–6619.
- (32) Hoertz, P. G.; Staniszewski, A.; Marton, A.; Higgins, G. T.; Incarvito, C. D.; Rheingold, A. L.; Meyer, G. J. Toward Exceeding the Shockley-Queisser Limit: Photoinduced Interfacial Charge Transfer Processes that Store Energy in Excess of the Equilibrated Excited State. *J. Am. Chem. Soc.* **2006**, *128*, 8234–8245.
- (33) Ferrere, S. New Photosensitizers Based upon [Fe(L)₂(CN)₂] and [Fe(L)₃] (L = Substituted 2,2'-Bipyridine): Yields for the Photosensitization of TiO₂ and Effects on the Band Selectivity. *Chem. Mater.* **2000**, *12*, 1083–1089.
- (34) Joya, K. S.; de Groot, H. J. M. Electrochemical *In Situ* Surface Enhanced Raman Spectroscopic Characterization of a Trinuclear Ruthenium Complex, Ru-red. *J. Raman Spectrosc.* **2013**, *44*, 1195–1199.
- (35) Joya, K. S.; Subbaiyan, N. K.; D'Souza, F.; de Groot, H. J. M. Surface-Immobilized Single-Site Iridium Complexes for Electrocatalytic Water Splitting. *Angew. Chem., Int. Ed.* **2012**, *51*, 9601.
- (36) Peter, L. M.; Wijayanthab, K. G. U.; Tahir, A. A. Kinetics of light-driven oxygen evolution at α -Fe₂O₃ electrodes. *Faraday Discuss.* **2012**, *155*, 309–322.
- (37) Barroso, M.; Mesa, C. A.; Pendlebury, S. R.; Cowan, A. J.; Hisatomi, T.; Sivula, K.; Gratzel, M.; Klug, D. R.; Durrant, J. R. Dynamics of Photogenerated Holes in Surface Modified α -Fe₂O₃ Photoanodes for Solar Water Splitting. *Proc. Natl. Acad. Sci. U.S.A.* **2012**, *109*, 15640–15645.
- (38) Zhong, D. K.; Choi, S.; Gamelin, D. R. Near-Complete Suppression of Surface Recombination in Solar Photoelectrolysis by “Co-Pi” Catalyst-Modified W:BiVO₄. *J. Am. Chem. Soc.* **2011**, *133*, 18370–18377.
- (39) Klahr, B.; Gimenez, S.; Fabregat-Santiago, F.; Bisquert, J.; Hamann, T. W. Photoelectrochemical and Impedance Spectroscopic Investigation of Water Oxidation with “Co-Pi”-Coated Hematite Electrodes. *J. Am. Chem. Soc.* **2012**, *134*, 16693–16700.

(40) Mills, T. J.; Lin, F.; Boettcher, S. W. Theory and Simulations of Electrocatalyst-Coated Semiconductor Electrodes for Solar Water Splitting. *Phys. Rev. Lett.* **2014**, *112*, 148304.

(41) Surendranath, Y.; Kanan, M. W.; Nocera, D. G. Mechanistic Studies of the Oxygen Evolution Reaction by a Cobalt-Phosphate Catalyst at Neutral pH. *J. Am. Chem. Soc.* **2010**, *132*, 16501–16509.

(42) Trotochaud, L.; Mills, T. J.; Boettcher, S. W. An Optocatalytic Model for Semiconductor–Catalyst Water-Splitting Photoelectrodes Based on In Situ Optical Measurements on Operational Catalysts. *J. Phys. Chem. Lett.* **2013**, *4*, 931–935.